Development and beam commissioning of a continuous-wave window-type radio-frequency quadrupole

P. P. Gan, K. Zhu,* Q. Fu, H. P. Li, M. J. Easton, Q. Y. Tan, S. Liu, S. L. Gao, Z. Wang, and Y. R. Lu†

State Key Laboratory of Nuclear Physics and Technology, Peking University, Beijing 100871, China

W. P. Dou, Q. Wu, C. Wang, Y. He, and H. W. Zhao

Institute of Modern Physics, China Academy of Science, Lanzhou 730000, China

(Received 6 December 2018; published 7 March 2019)

The radio-frequency quadrupole (RFQ) group at Peking University has built a window-type RFQ, operating at 162.5 MHz in continuous-wave (cw) mode. It is designed to accelerate a 50 mA deuteron beam from 50 keV to 1 MeV with a vane length of 1.809 m. The cavity was fabricated in two segments using 100% oxygen-free electronic (OFE) copper. Using an iterative assembly and measurement procedure for the precise alignment of the two segments, we reduced the assembly errors to within ± 0.05 mm. The radio frequency (rf) measurements of the whole cavity show excellent rf properties, with the measured intrinsic Q-value of 8962, which equates to 96% of the simulated value for OFE copper. We also investigated field fluctuations caused by misalignment between the two segments, and studied their impact on the beam transmission using beam dynamics simulations. During field tuning, we compiled a set of unique tuning rules for the window-type RFQ. After tuning, the maximal field unflatness of the single quadrant is within $\pm 2\%$, and the asymmetry of the four quadrants is within $\pm 1\%$. During rf conditioning, the cw power of the cavity reached 55 kW within 32 hours, and we have recorded nearly seven hours of stable running at a cw power of 50 kW. The measured bremsstrahlung spectrum shows that the accelerator needs 49.9 kW to generate the intervane voltage of 60 kV, with a specific shunt impedance of 130.5 kΩ m. An H_2^+ ion beam extracted from an electron cyclotron resonance ion source was used for the beam commissioning, because deuteron beam acceleration will bring a serious radiation field. We achieved stable and robust acceleration of about 1.5 mA cw H_2^+ beam for one hour.

DOI: 10.1103/PhysRevAccelBeams.22.030102

I. INTRODUCTION

High-current continuous-wave (cw) RFQs are a research hot spot in the field of linear accelerators, as they can be applied to fusion material irradiation, accelerator driven subcritical systems, nuclear waste transmutation and nuclear fuel proliferation, radioactive nuclear beam production and compact high-intensity neutron source. In recent decades, several high-current cw RFQs have been built, such as the IFMIF RFQ [1], C-ADS injector-II RFQ [2], SARAF RFQ [3] and the LEDA RFQ [4]. Most of these RFQs are at the experimental stage, with no full cw power operation or with limited cw operation time. Therefore, the realization of a high-current cw RFQ is still a significant challenge. The most common problems for cw RFQs are [5]: sparking or multipacting at higher power; overheated spots at problem location such as the couplers, tuners, or contact fingers; detuning due to beam loading, rf heating and lost beam heating.

Since 2013, Peking University (PKU) and the Institute of Modern Physics (IMP) have been collaborating on a new "973" project, which aims to accumulate experience in design and fabrication of high-current cw RFQs and promote their development by building a 50-mA cw deuteron RFQ. The problems for cw RFQs mentioned above provide a lot of valuable lessons for our RFQ design. We have already completed the beam dynamics design and the rf structure design [6,7]. The main parameters of this RFQ are listed in Table I. We optimized the beam dynamics design to control the limiting current from the gentle bunching section to the end of the acceleration section, and adopted a matched and equipartitioned design method to reduce the radius of the transverse envelope, suppress the

*Corresponding author.
zhukun@pku.edu.cn
†Corresponding author.
yrlu@pku.edu.cn

TABLE I. Main parameters of the window-type RFQ.

Parameter	Value
Operating frequency [MHz]	162.5
Particle	D^+
Beam current [mA]	50
Duty factor	100%
Input/output energy [MeV]	0.05/1.03
Intervane voltage [kV]	60
Length of the vanes [m]	1.809
Cavity radius [mm]	170.00
Intrinsic quality factor (simulated)	9300
Power (simulated) [kW]	48.9
Kilpatrick coefficient	1.67
Pole tip radius [mm]	2.57–3.32
Average aperture [mm]	3.88
Mode separation between TE_{210} and TE_{110} (simulated) [MHz]	2.99

increase of the emittance, and reduce the beam loss at high-energy section. The RFQ copper cavity is shown in Fig. 1. It adopts a window-type structure which is more compact than the traditional four-vane structure. We achieved low power consumption and sufficient mode separation with this design.

Several window-type RFQs have completed rf or beam commissioning, such as the TWAC RFQ [8], ATLAS RFQ [9,10] and the RFQ for NICA [11]. They operate at lower frequencies and are designed to accelerate heavy ions. So far, only the ATLAS RFQ has realized cw running. Our RFQ will be the first high-frequency window-type cw RFQ.

In this paper, Sec. II presents the fabrication, rf measurement and tuning results of the window-type cavity; Sec. III describes the setup of the two couplers and high power test of the cavity; Sec. IV demonstrates the beam commissioning results, and the comparison with other cw deuteron RFQs is given in Sec. V.

II. FABRICATION AND LOW POWER EXPERIMENT

A. Fabrication and measurement

For high-current cw RFQ accelerators, the successful transmission and acceleration of the beam is highly influenced by the accuracy of the machining and assembly process. Our design parameters require a precision better than 0.05 mm.

As can be seen in Fig. 1, the RFQ cavity consists of two almost identical segments and end plates, which are all made of oxygen-free copper. Each segment is 904.50 mm long, and is divided into four vanes and four cavity walls for manufacturing. The RFQ is equipped with 28 tuners, with a diameter of 60 mm, as well as two couplers, eight vacuum ports, eight pickups and 56 cooling connectors. The reason why we need so many tuners is that because of the design of varying pole tip radius, the original electric field along the RFQ is relatively rough, and 16 tuners with 50-mm diameter are not enough for field tuning as discussed in Ref. [7]. The fabrication procedure includes the following main stages: (i) preliminary machining of vanes, cavity walls and end plates; and drilling of water-cooling channels; (ii) semifinishing and fine machining; (iii) hydrostatic pressure testing of the cooling channels; (iv) assembly of each segment, frequency check of individual segments; followed by disassembly of segments and cleaning of all parts; (v) assembly and final brazing; (vi) postbrazing machining, rf measurement, final cleaning and vacuum leak checking of each segments; (vii) assembly of the segments and end plates, and installation of external water-cooling pipes and vacuum system components.

In order to ensure the high precision, we performed coordinate measuring machine (CMM) measurements of all components at various stages of the manufacturing process. We used ball-end milling tools to process the vane modulations, as the RFQ was designed with variable

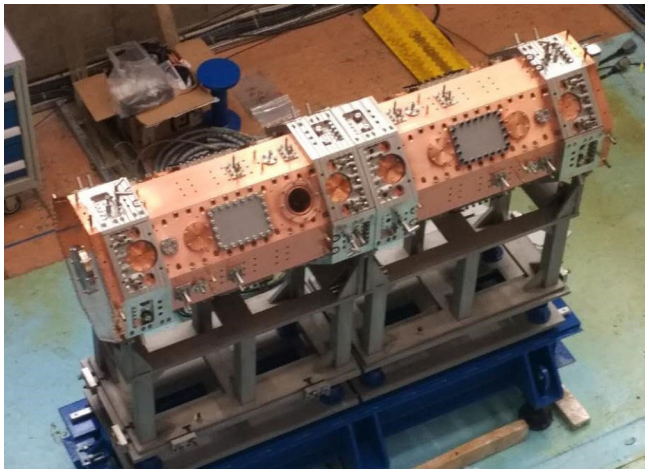

FIG. 1. View of the whole window-type RFQ cavity.

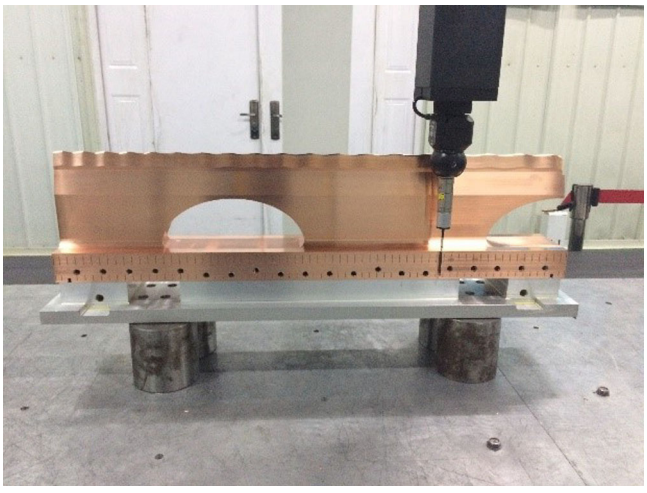

FIG. 2. Machining error measurement of the electrodes.

TABLE II. Maximum machining errors of the electrodes (unit: mm).

Electrodes	Segment No. 1	Segment No. 2
Vertical electrode I	0.030	0.019
Vertical electrode II	0.031	0.034
Horizontal electrode I	0.024	0.027
Horizontal electrode II	0.027	0.032

transverse radius of the vane tips. Figure 2 shows the machining error measurement of the electrodes. The results are listed in Table II. The maximum machining error is 0.034 mm, located at the vane tip.

We assembled the RFQ components vertically, as shown in Fig. 3. During the test of each segment, we adopted a method combining CMM measurement and electric field distribution measurement to ensure high-accuracy assembling. The measured electric field distribution of the four quadrants can directly reflect the symmetry of the cavity. We measured the field distribution once we assembled one segment, and then performed the next adjustment based on the measurement results. This process is repeated until the field distribution and the CMM measurement meet our requirements. After properly adjusting the vanes, we measured the transverse assembling errors to be within ± 0.05 mm at both ends of each segment. The two segments were brazed and postprocessed successively. Their vacuum levels reached 1×10^{-5} Pa. Next, we used a laser tracking system to align the two segments. The transverse alignment error was -0.03 mm. Finally, we achieved a machining precision and an assembly precision better than 0.05 mm, well within the targets set for this RFQ.

B. rf measurement and tuning

After the segments were joined together, we measured the rf characteristics of the whole RFQ cavity using two pickups in transmission mode with very weak coupling. As shown in Table III, the measured results are close to those predicted by CST [12] simulations. The operating frequency of the whole RFQ without tuning and power-input loops is 0.233 MHz below the simulated value. The measured Q_0 of the operating mode is 96% of the simulated value.

Figure 4 shows the 20-mm off-axis electric field distributions of the four quadrants after primary collimating. There is a clear step in the middle of the cavity, at the location of the electrode seams between the two segments, as shown in Fig. 5. This electric field step is caused by the assembling error of the two segments—especially the transverse alignment error.

As this electric field step may affect the beam transmission, it is necessary to study it through beam dynamics simulations. However, from the distribution of the electric field, we cannot determine the nature of the alignment error. To simplify the simulations, we studied the transmission efficiency and acceleration efficiency under two separate error conditions: a translation at 45 degrees to the vane direction, and a rotating shift of the second segment. The acceleration efficiency is a parameter to describe how many particles are accelerated to the designed energy. The simulation results, obtained using TOUTATIS [13], are shown in Fig. 6. As it is difficult to characterize the rotation of electrodes in TOUTATIS, we use the way that the electrode is shifted in Fig. 6(b) to represent rotation, using two translation effects. The first type of translation results in a deviation of the central axis of the second cavity, and as the shift value increases, the transmission efficiency reduces with a relatively slow speed. The second rotation shift does not cause a change in the central axis, but maintains the symmetry of the four electrodes. Only when the shift exceeds 0.20 mm, the transmission efficiency begins to decrease significantly. Therefore, the effect of our transverse alignment error on the transmission efficiency of the beam is not more than 1%.

Tuning of the RFQ includes adjusting the cavity frequency and the electric field distribution. Figure 7 illustrates the positions of the tuners relative to the coupling windows and the magnetic field distribution. Figure 8 shows the effect on the cavity frequency of inserting tuners

FIG. 3. Single cavity assembly process and assembling error measurement.

TABLE III. Comparison of the simulated and measured rf parameters of the cavity.

	Simulated				Measured			
Mode	Frequency [MHz]	Intrinsic quality factor[a]	Frequency [MHz]	Intrinsic quality factor[a]	Loaded quality factor[a]	S_{21} [dB]	S_{11} [dB]	S_{22} [dB]
TE_{210}	161.930	9300	161.697	8962	7952	−18.68	−1.32	−0.89
$^{0}TE_{110}$	164.922	10427	164.664	10022	8654	−16.80	−1.51	−1.24
TE_{211}	177.840	5933	177.200	5916	5764	−31.84	−0.30	−0.15
$^{\pi}TE_{110}$	180.548	4298	182.645	4241	3896	−21.40	−0.85	−0.69
$^{0}TE_{111}$	183.273	4667	185.447	3349	3138	−23.73	−0.67	−0.50

[a]The electric conductivity of copper is adopted as $\sigma = 5.0 \times 10^7$ S/m.

1–7 of the first quadrant to different depths in turn, and the change of the cavity frequency can be measured, as shown in Fig. 8. The seven curves are almost resolved into three curves, demonstrating that the tuning capabilities fall into three distinct tuning rates (1.48, 2.38, and 2.88 kHz/mm).

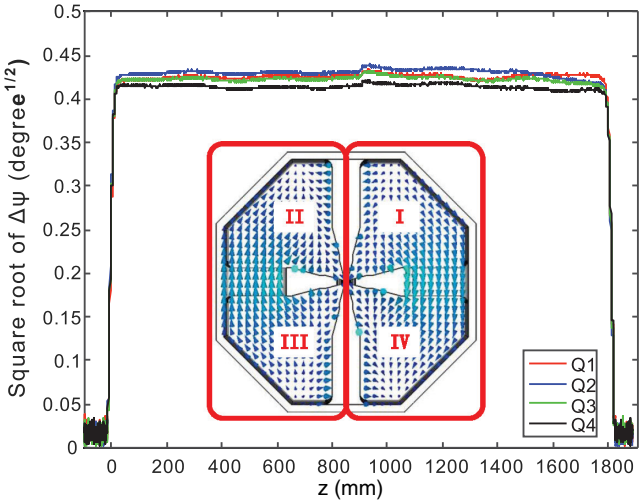

FIG. 4. Electric field distributions of the four quadrants after primary collimating.

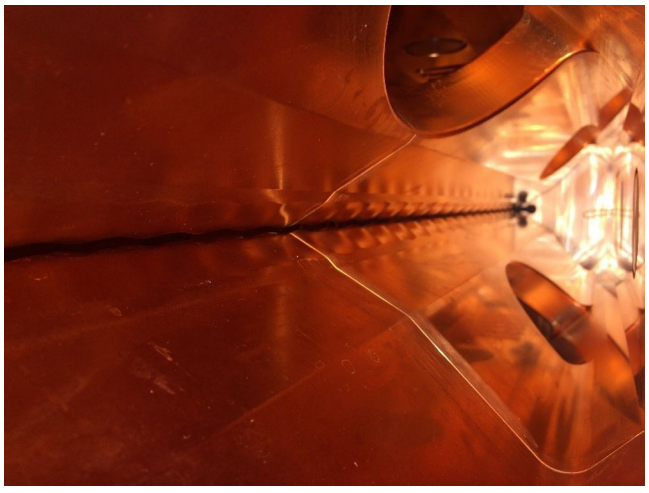

FIG. 5. View of the electrode seams between the two segments.

This is because the magnetic field varies periodically with the coupling windows and the tuners in different longitudinal positions correspond to different magnetic field values (see Fig. 7).

Through simulation, we obtained the effect of the tuner at different positions on the four-quadrant electric field. Figure 9 shows the effect of 60-mm insertion of tuner 1 and

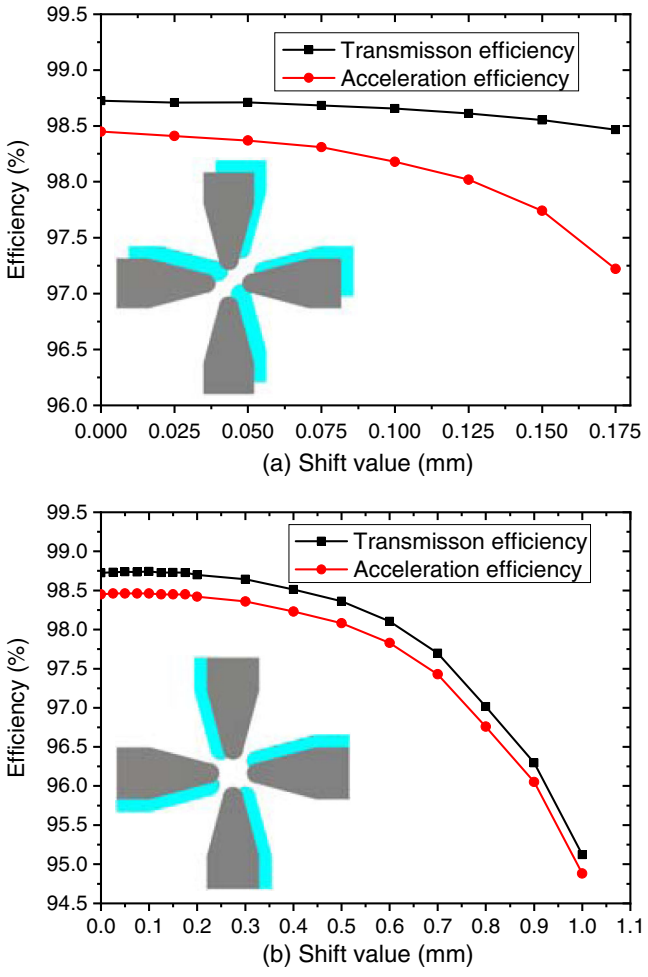

FIG. 6. Simulated transmission and acceleration efficiency under the effect of alignment errors of the second cavity: (a) 45-degree shift and (b) rotating shift.

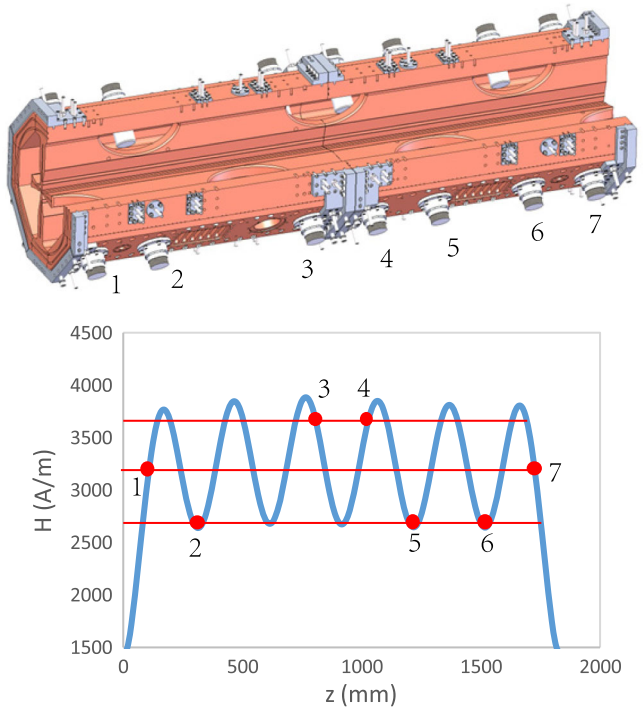

FIG. 7. Positions of tuners relative to (top) the coupling windows and (bottom) the magnetic field distribution.

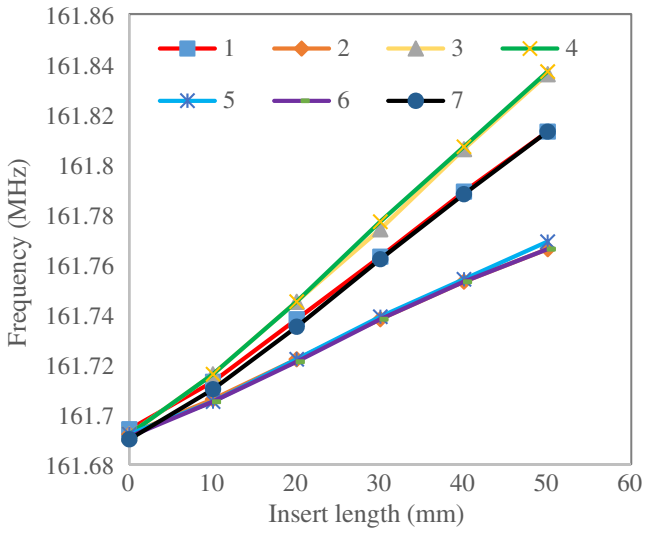

FIG. 8. Cavity frequency as a function of the inserted length of each tuner in quadrant I.

tuner 3 in the first quadrant on the electric field distribution of the four quadrants. Because of the half-window structure at the end of the horizontal electrodes, quadrants I and IV, and quadrants II and III are strongly coupled together, respectively. On the other hand, because of the windows in the vertical electrodes, quadrants I and II, and quadrants III and IV are weakly coupled together, respectively. Adjusting tuner 1, because the end coupling effect is strong, the electric field of the mutually strongly

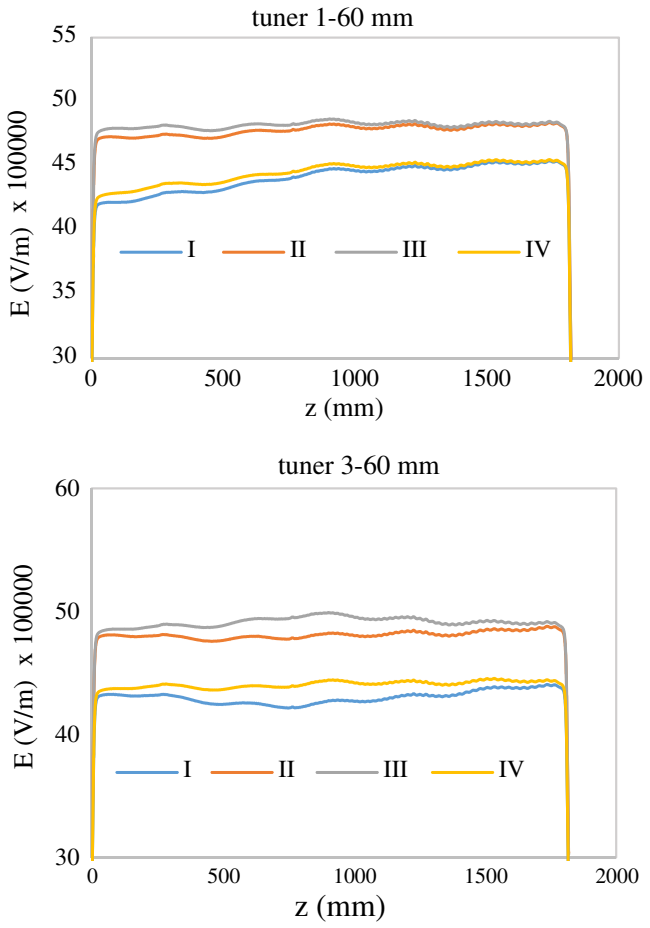

FIG. 9. Effect of 60 mm insertion of tuner 1and tuner 3 in the first quadrant on the electric field distribution of the four quadrants (under 1 J stored energy).

coupled quadrants moves almost together. While adjusting tuner 3, the coupling effect of the strongly coupled quadrants is not so obvious. Thereby, to tune the asymmetry between the strongly coupled quadrants, tuners 3 and 4 are the most effective.

We carried out the tuning of the entire cavity based on the above considerations. In terms of electric field tuning, the aim of tuning is to adjust the unflatness of the field in each quadrant and the asymmetry of the four quadrants to within ±1%; in terms of frequency tuning, as the cavity frequency will be reduced due to the thermal expansion of the cavity under high power conditions, we calculated that the cavity frequency should be tuned to 162.75 MHz.

The unflatness of the field and the asymmetry of four quadrants were calculated according to the following two formulas, respectively:

$$\text{Unflatness} = \frac{E_{Qk} - \overline{E_Q}}{\overline{E_Q}} \times 100\%,$$

$$\text{Asymmetry} = \frac{E_{Qk} - \overline{E_k}}{\overline{E_k}} \times 100\%. \quad (1)$$

Here the subscript Q ($Q = I, II, III, IV$) is the quadrant label, and the k ($k = 1, 2, 3, \ldots$) is the point number that refers to different longitudinal position along the cold model. Thus, $\overline{E_Q}$ is the average electric field of a quadrant, and $\overline{E_k}$ is the average of four quadrants' field at a longitudinal position.

Before tuning, as shown in Fig. 10, the maximum unflatness of the field in each quadrant ranges from $+3.04\%$ to -2.61%, and the asymmetry of the four quadrants ranges from $+2.95\%$ to -2.61%. It indicates that the initial state is good and the target mentioned before can be achieved without too many adjustments. During the tuning process, tuners 3 and tuner 4 play an important role in adjusting the asymmetry between the strongly coupled quadrants, which confirms the tuning rules we obtained from the simulations.

After tuning, we measured the frequency as 162.745 MHz, and the Q_0 value as 8019 (tuner and end plate are aluminum). As shown in Fig. 11, excluding the electric field step discussed above, the maximum unflatness of the field in each quadrant ranges from $+1.53\%$ to -1.28%, and the asymmetry of the four quadrants ranges from $+0.91\%$ to -0.77%. Furthermore, the electric field distribution of the four quadrants is very similar to the simulated field distribution, including the fluctuations caused by the magnetic coupling windows and the modulations of the acceleration section, as shown in Fig. 12.

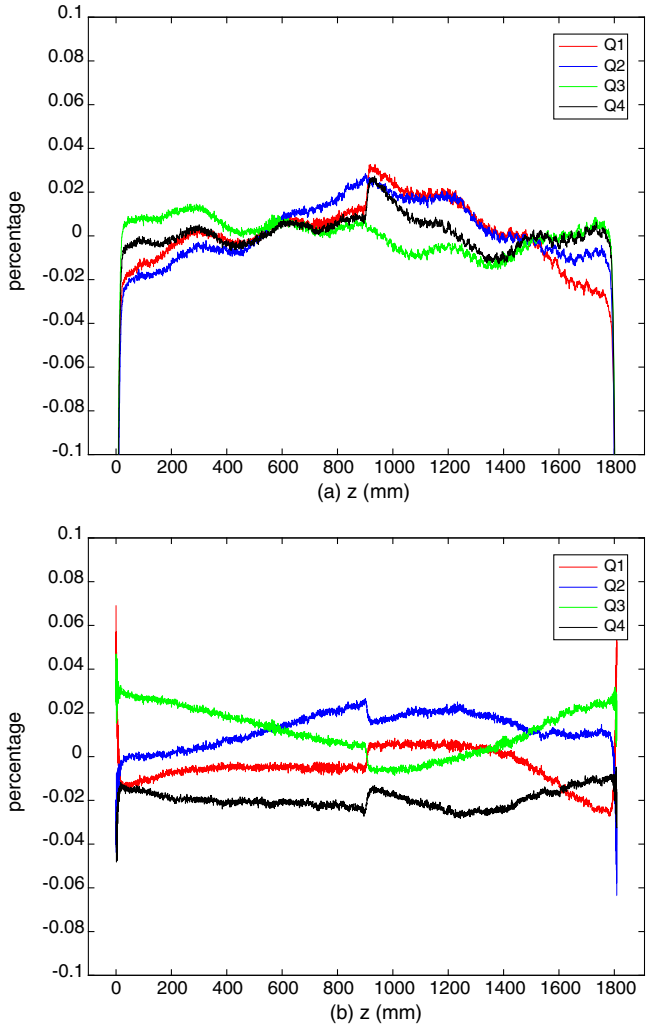

FIG. 10. (a) The unflatness of the field in each quadrant and (b) the asymmetry of the four quadrants at frequency of 161.688 MHz before tuning.

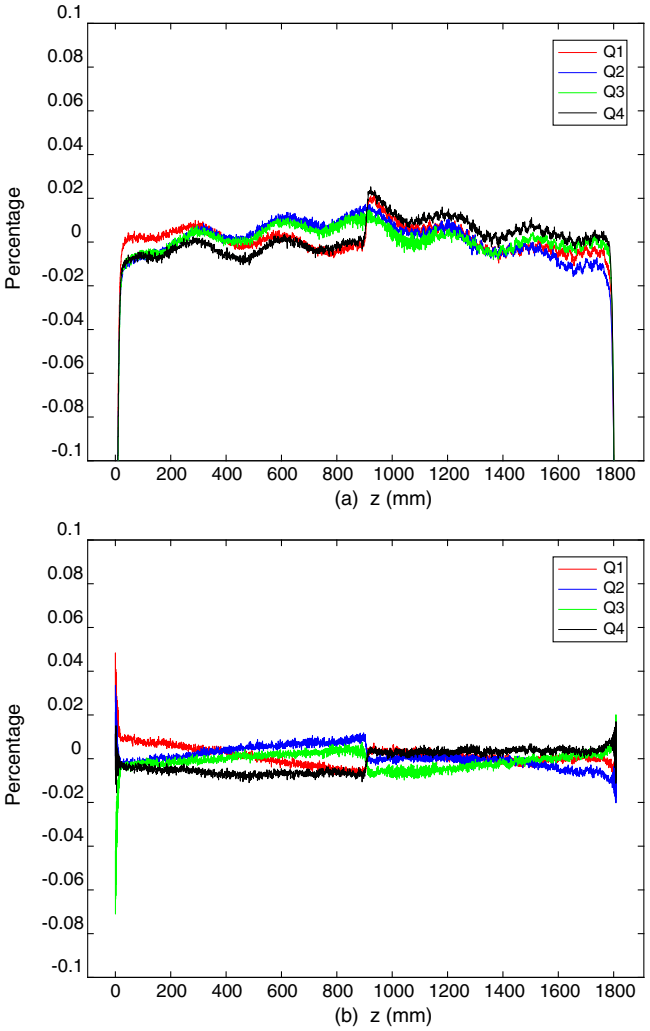

FIG. 11. (a) The unflatness of the field in each quadrant and (b) the asymmetry of the four quadrants at frequency of 162.745 MHz after tuning.

III. rf CONDITIONING

A. Coupler setup

The RFQ uses two couplers for rf input. Before rf conditioning, we needed to set the coupling factor to the target value by rotating the couplers. In order to leave enough margin for adjustments, the loop area of the coupler is 725.6 mm^2, larger than the simulated required value of

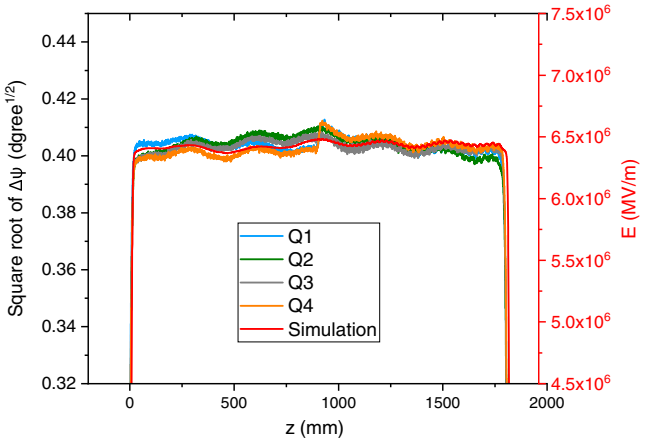

FIG. 12. Comparison of measured and simulated electric field distributions after tuning.

575 mm^2. We were told that the maximum beam current that can be extracted from the ion source is 20 mA. This means that the total coupling factor needed to be set as 1.4, that is, each coupler should be 0.7. It should be noted that for a two-port network, the measured coupling factor is not the true value. This is because that looking from one coupler port, the other coupler port is equivalent to connect a load resistance of 50 Ω. The intrinsic quality factor Q_0 becomes loaded quality factor Q_L. According to the definition of the coupling factor, the measured coupling factors of a two-port network are given by

$$\beta_1^* = \frac{Q_{L2}}{Q_{ex1}} = \frac{1}{\frac{1}{Q_0}+\frac{1}{Q_{ex2}}}\cdot\frac{1}{Q_{ex1}} = \frac{\beta_1}{1+\beta_2} \tag{2}$$

$$\beta_2^* = \frac{Q_{L1}}{Q_{ex2}} = \frac{1}{\frac{1}{Q_0}+\frac{1}{Q_{ex1}}}\cdot\frac{1}{Q_{ex2}} = \frac{\beta_2}{1+\beta_1}, \tag{3}$$

where β_i and β_i^* are the true and measured coupling factor of the i port.

Therefore, the true coupling factors can be derived by [14]

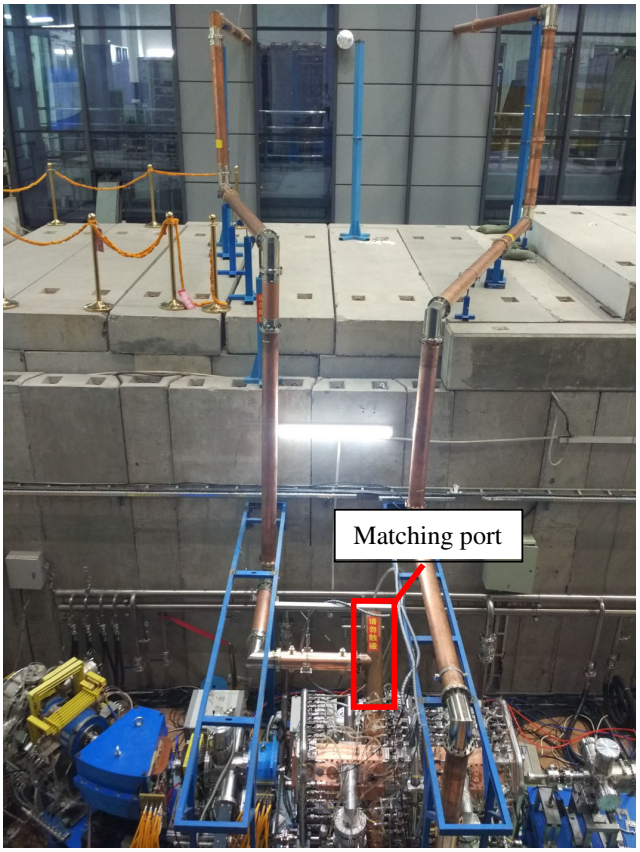

FIG. 13. The power feed system.

$$\beta_1 = \frac{\beta_1^*(1+\beta_2^*)}{1-\beta_1^*\beta_2^*}, \qquad \beta_2 = \frac{\beta_2^*(1+\beta_1^*)}{1-\beta_1^*\beta_2^*}. \tag{4}$$

We measured the coupling factor with and without matching ports included. The measurement results are listed in Table IV. Without matching ports, the frequency of the cavity was 162.732 MHz, and the Q_0 value was 8643. This is significantly larger than reported in Sec. II B above, because the end plates and tuners were now replaced with copper versions. The matching port (see Fig. 13) is a quarter wave of EIA 6 1/8" coaxial waveguide, with its own resonance frequency. If there is a mismatch with the RFQ cavity, it will have an impact on the measured results.

TABLE IV. Measurement results for the two couplers.

	Without matching ports		With matching ports	
Two ports	Coupler I (in)	Coupler II (out)	Coupler I (in)	Coupler II (out)
S_{11} or S_{22} [dB]	−7.52	−7.55	−7.28	−7.24
Measured coupling factor	0.407	0.409	0.396	0.394
Real coupling factor	0.690	0.691	0.655	0.652
Loaded quality factor Q_L	3630		3716	
Intrinsic quality factor Q_0	8643		8571	
Frequency [MHz]	162.732		162.833	

As can be seen from Table IV, the frequency shifts to 162.833 MHz after the matching ports are connected to the couplers.

B. High power test

The RFQ is driven by two solid-state rf amplifiers of 80 kW through two couplers, as shown in Fig. 13. We developed a control system to monitor the RFQ operation, including two vacuum gauges, two pickup loops, two arc detectors and 30 sets of thermometers and flow meters. The rf conditioning started at the cavity vacuum level of 1.9×10^{-6} Pa and was performed in cw mode.

After about 32 hours of effective conditioning, cw power up to 55 kW was transmitted into the RFQ. During the conditioning, the only problems triggered were occasional vacuum and power reflection protection trips, and no sparks were detected by the arc detectors. The RFQ had operated for 1 hour and 25 minutes in 55 kW cw mode before a spark occurred. Additionally, we recorded over seven hours of uninterrupted (no-spark) operations at cw power of 50 kW, as shown in Fig. 14. These results indicate that the RFQ cavity design was successful and it can run stably in high power cw mode.

Figure 15 shows the change of frequency with cavity power. It can be seen that the frequency decreases almost linearly with the cavity power, with a slope of 2.8 kHz/kW.

C. Intervane voltage measurement

We carried out the intervane voltage calibration using x-ray spectrum measurements. The high voltage between the intervanes leads to field emission, and these emitted electrons are accelerated to the energy corresponding to RFQ voltage and bombard the copper vanes, resulting in Bremsstrahlung x-ray emission, the maximum energy of these x rays corresponds to the vane voltage. We used a CdTe spectrometer for the measurements of x-ray spectra.

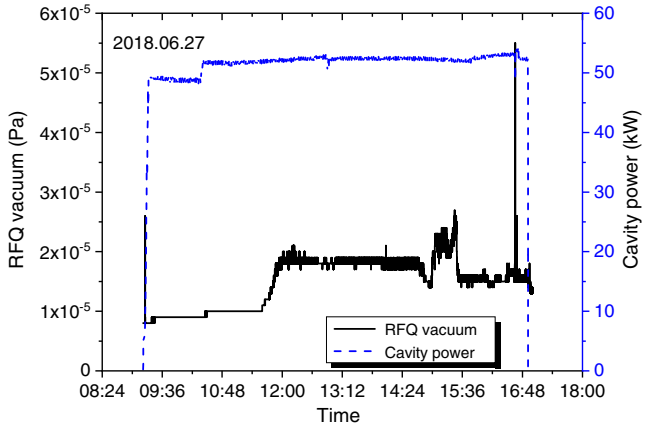

FIG. 14. Uninterrupted (no-spark) operations at cw power of 50 kW recorded over 7 hours.

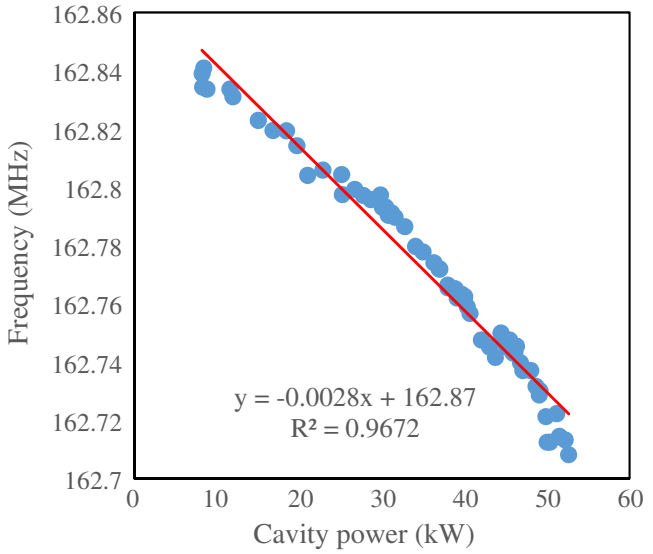

FIG. 15. Frequency of the RFQ as a function of cavity power.

It was calibrated with ion-55 and amercium-241 sources, as shown in Fig. 16.

We added a special quartz window to the RFQ to allow the x rays to reach the spectrometer. The spectrometer was mounted directly facing the intervane gap, as shown in Fig. 17. In order to attenuate the high intensity of the x rays, we covered the quartz window with a 3-mm-thick circular copper plate.

Figure 18 shows a typical x-ray spectrum corresponding to the RFQ voltage. There are different methods to quantify the cutoff energy of the x rays [15–17]. As our measured spectra are smooth and clean, we used linear fitting with a beveled edge for the high energy region, and took the horizontal intercept as the cutoff energy. We measured the intervane voltage under different cavity power conditions, at three separate times. Figure 19 shows the results. The specific shunt impedance of the RFQ can be deduced from the slope of the linear fitting line. The average value of the three measurements of the specific shunt impedance is 130.5 kΩ m, which is 93% of our simulated value.

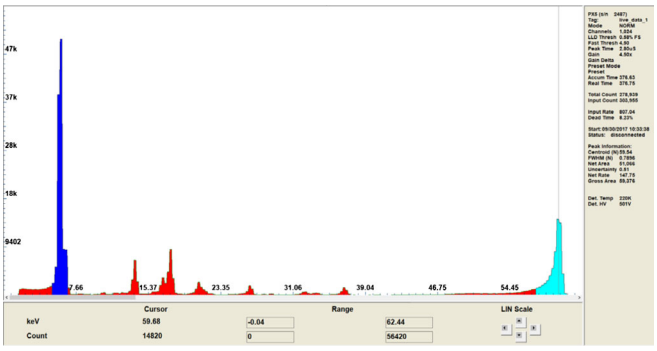

FIG. 16. Spectrometer calibration with ion-55 and amercium-241 sources.

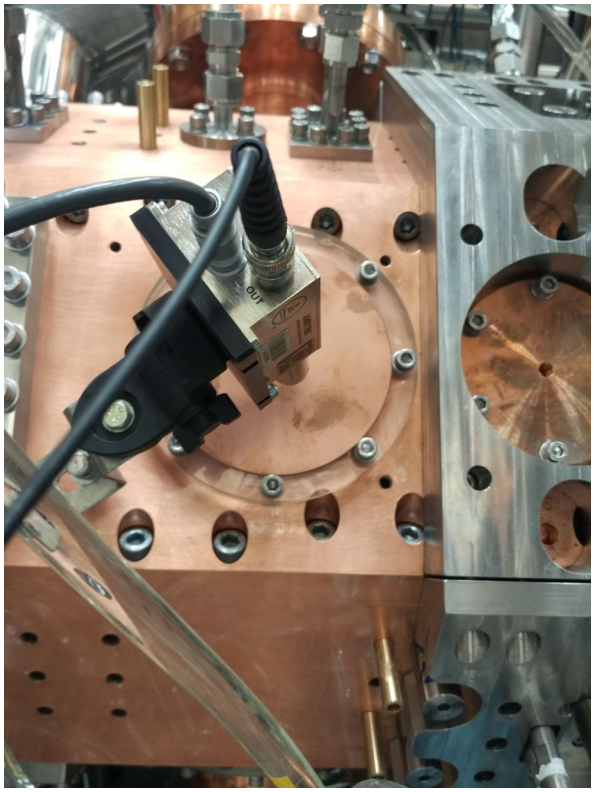

FIG. 17. Location of the quartz window and spectrometer.

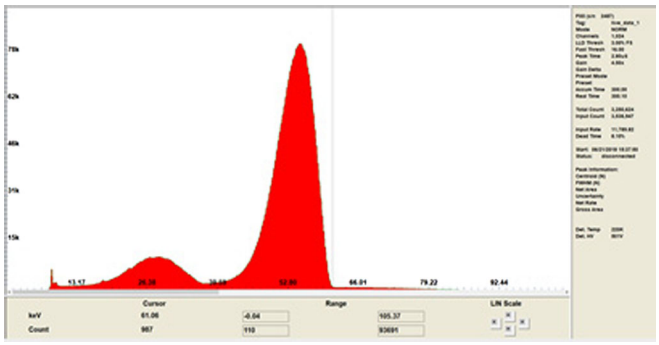

FIG. 18. X-ray spectrum corresponding to the 61 kV intervane voltage.

Calculated from the measured specific shunt impedance, an intervane voltage of 60 kV corresponds to a cavity power of 49.9 kW, which is very close to the simulated value of 48.9 kW.

IV. BEAM COMMISSIONING

The experimental setup for beam commissioning of the RFQ is shown in Fig. 20. It consists of an electron cyclotron resonance (ECR) ion source, a low energy beam transport (LEBT) system based on three solenoids and a 32.5° bending magnet, the RFQ and a medium energy beam transport (MEBT) section. Between the Solenoid 3 and the

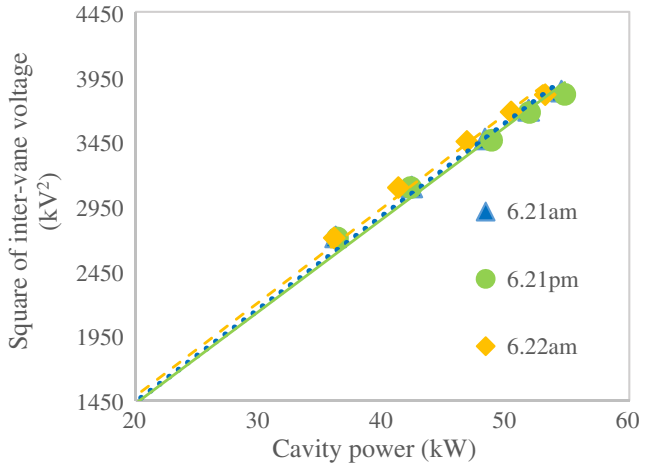

FIG. 19. Square of intervane voltage as a function of cavity power.

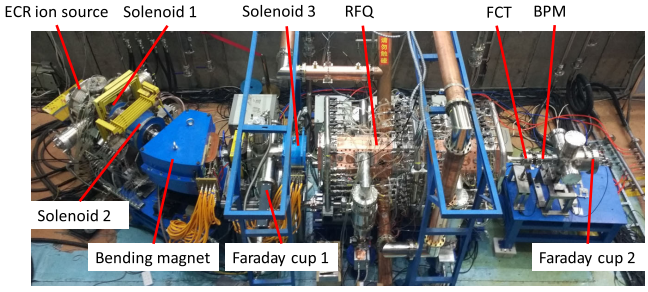

FIG. 20. Overview of the RFQ test area.

RFQ, there is a chopper used to provide pulsed beam for beam commissioning. Two water-cooled Faraday cups (FCs) were used for transmission measurement. The bias voltage of FC1 and FC2 were set to −300 and −800 V, respectively, to suppress secondary electron yield (SEY). A fast current transformer (FCT) and a beam position monitor (BPM) were installed after the exit of the RFQ for beam energy measurement. The extraction voltage of the ion source was fixed at 50 kV to provide the design injection energy of 50 keV for the H_2^+ test beam.

A. Energy measurement

We measured the beam energy of the RFQ using the time-of-flight (TOF) method. Figure 21 shows the distance between the FCT and BPM, and the corresponding time signals. The flight time of the beam over the distance of 180.0 mm is greater than double the rf period and less than triple the rf period. So, the flight time is equal to the sum of double the rf period and the time difference between the two signals. The error in the energy measurement can be calculated from the errors in the length and time measurements. The measurement tolerance of our timing system is 51.25 ps. According to the error transfer formula, the error in our energy measurement is ±0.01 MeV. We made ten

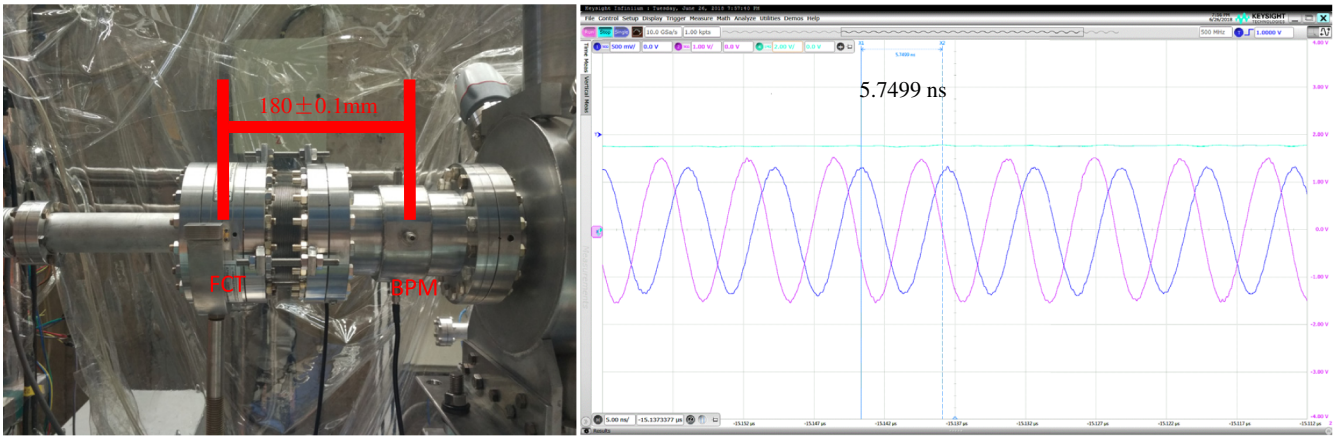

FIG. 21. Measured distance and beam signals detected by the FCT and BPM (the FCT signal is blue, the BPM signal is pink).

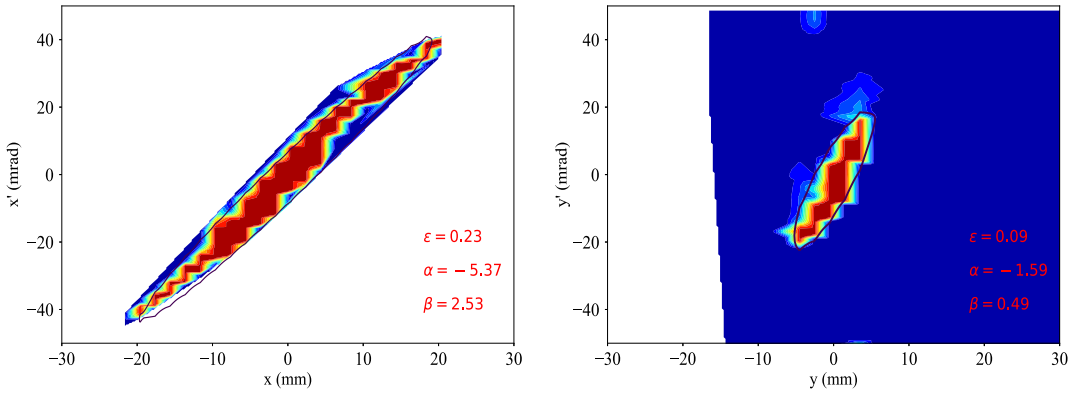

FIG. 22. Beam phase space at the measurement location.

measurements, and the averaged output energy of the RFQ is 1.04 ± 0.01 MeV, which is consistent with the simulated value of 1.03 MeV.

B. Beam transmission measurement

We measured the beam emittance at the location of the first Faraday cup (FC1, see Fig. 20). Under the optimized parameters of the three solenoids, the measured phase-space distribution of the beam shows significant asymmetry in the x and y directions after the bending magnet, as shown in Fig. 22. Meanwhile, it can be noticed that the phase-space beam distribution also shows asymmetry in the x direction. The asymmetry can be divided into two aspects, the displacement in the x direction and the slight distortion of the beam. The former is caused by the collimation of the bending magnet, the latter is leaded by nonlinearities of the nonparaxial region of the solenoid 1 and solenoid 2. The Twiss parameters relative to the ellipse are used in transmission simulation. From the measurement location to the second Faraday cup (FC2, see Fig. 20), the simulated transmission efficiency, obtained using TraceWin code [18], is about 95% for a 1.5 mA beam. The measured transmission efficiency was $90.6\% \pm 1.8\%$ for a 1.5 mA pulsed beam. We suspected that part of the beam struck to the electrodes of the chopper because the current on the electrodes changed when beam passing by. Table V shows the comparison between the designed and measured Twiss parameters at the RFQ input and their

TABLE V. Comparison between the designed and measured Twiss parameters at the RFQ input and their corresponding transmission efficiencies.

	α	β [mm/mrad]	$\varepsilon_{\mathrm{nor,rms}}$ [πmm · mrad]	Transmission [%]
Design	1.34	0.06	0.20	98
Measured in x direction	1.21	0.09	0.22	95
Measured in y direction	0.82	0.03	0.40	

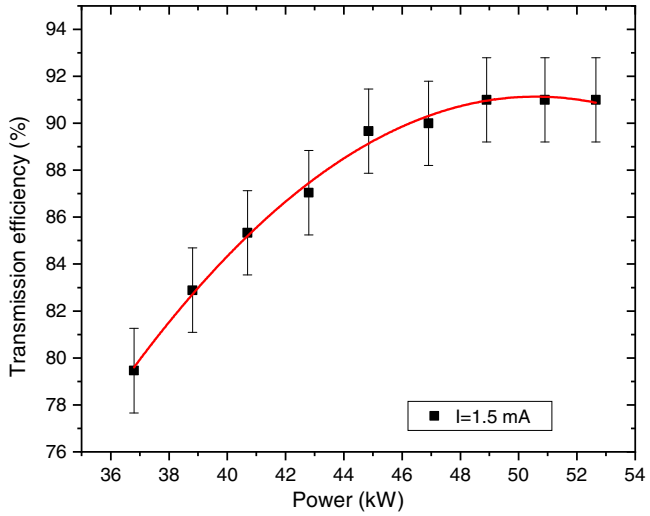

FIG. 23. Transmission efficiency as a function of RFQ cavity power.

corresponding transmission efficiencies. The measured one is actually deduced from the measured phase space shown in Fig. 22, using TraceWin code. It can be seen that the mismatch of the Twiss parameters can cause beam loss to some extent.

The experimental results for the pulsed-beam transmission under different RFQ cavity power are plotted in Fig. 23. The transmission efficiency remains almost constant for an input power greater than power of 49 kW.

After obtaining these pulsed-beam results, we switched the RFQ into cw mode. Figure 24 shows the beam current at FC1 and FC2 during one hour of cw operation at a cavity power of 50 kW. Due to sparks in the ECR ion source, the FC2 beam current drops off three times. Figure 25 shows the vacuum level of the LEBT, RFQ and beam dump during this one hour of cw operation. The RFQ vacuum is mostly stable at 8×10^{-6} Pa. The beam dump vacuum increased to

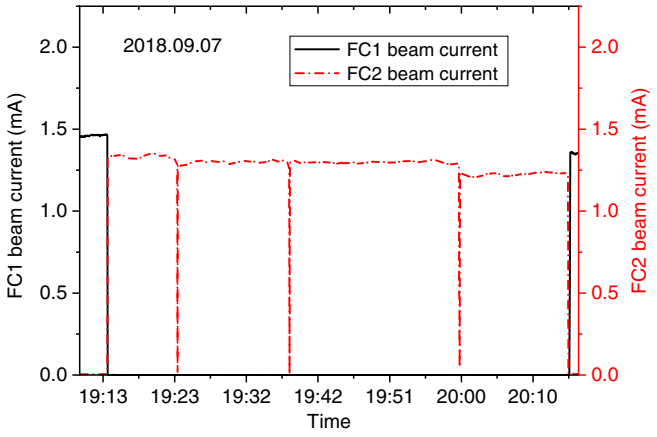

FIG. 24. Change of FC1 and FC2 beam current during one hour of cw operation.

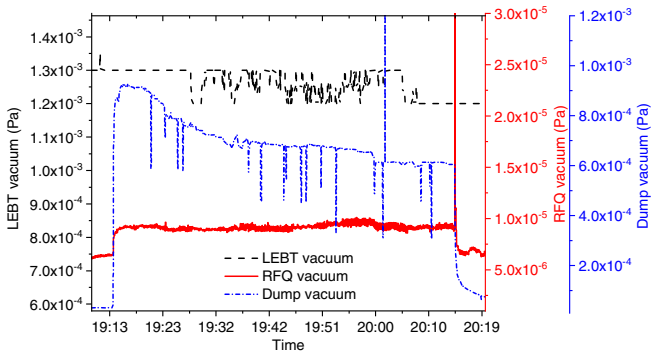

FIG. 25. Change of vacuum in LEBT, RFQ and beam dump during one hour of cw operation.

1.25×10^{-3} Pa, then, gradually fell down. This is because there is an outgassing process when the beam bombards the Faraday cup. During cw running, the maximum temperature rise of the cooling water in FC2 is 3.6°C, which is equivalent to absorbing power of 1.2 kW, roughly consistent with the beam power. Additionally, the transmission efficiency of the cw beam does not vary much in the range from 1.5 to 2 mA, with an average of over 90% transmission, as shown in Table VI.

V. COMPARISION WITH OTHER DEUTERON RFQ

There are currently five cw deuteron RFQs in the world. The main parameters of these RFQs are listed in Table VII. The SPIRAL2 RFQ, working at a low frequency of 88 MHz, is designed to accelerate heavy ions. Although it has demonstrated 1.34 mA He^{2+} cw running with 98.5% transmission efficiency, it has not achieved its target performance levels (cw, 113.6 kV). The rest of these RFQs operate at higher frequencies. The SARAF phase I RFQ has achieved acceleration of a 1.15 mA deuteron beam in quasi-cw mode. However, the transmission is only around 70%. The IFMIF RFQ and CMIF RFQ have completed beam commissioning in pulse mode, and are on their way to cw running. Our 973 RFQ is the first high-frequency window-type RFQ, and it has successfully accelerated a 1.78 mA H_2^+ cw beam with 91.3% ± 1.8% transmission efficiency.

TABLE VI. Transmission efficiency of cw beam under cavity power of 49.7 kW.

FC1 beam current [mA]	FC2 beam current [mA]	Transmission [%]
1.53	1.38	90.2
1.65	1.48	89.7
1.67	1.51	90.4
1.95	1.78	91.3

TABLE VII. Main parameters of the deuteron cw RFQ in the world.

Project	Type	Frequency (MHz)	Designed beam current (mA)	Intervane voltage (kV)	E_{in}/E_{out} (MeV)	Length (m)	Status and transmission efficiency
SPIRAL2 [19,20]	4 vane	88	5	80	0.04/1.5	5.08	cw 1.34 mA He^{2+} 98.5%
SARAF [21]	4 rod	176	5	56	0.04/3	3.72	cw 1.15 mA $D^+ \sim 70\%$
IFMIF [22,23]	4 vane	175	130	79–132	0.1/5	9.78	Pulse 13 mA H^+
CMIF [24]	4 vane	162.5	10	65	0.04/3	5.26	Pulse 8.04 mA H_2^+ 97.6%
973 RFQ	window	162.5	50	60	0.05/1	1.81	cw 1.78 mA H_2^+ 91.3%

VI. SUMMARY

We have constructed and tested the first high frequency window-type cw RFQ. The fabrication and assembly of the RFQ achieved high precision. For the low power test, the experimental and simulated results show good agreement. New coupling rules between quadrants are summarized and used to guide the field tuning. The rf conditioning results have indicated a successful rf structural design. For the beam commissioning, H_2^+ beam was accelerated to 1.04 MeV. The transmission efficiency from FC1 to FC2 is over 90% for cw beam of 1.5–2 mA. Most recently, one hour of stable cw operation has been successfully demonstrated. These results illustrate the great success of this cw RFQ. The experience of the design and fabrication can be applied to future cw RFQs.

ACKNOWLEDGMENTS

Many thanks to the members of RFQ group at Institute of Modern Physics who have given lots of helps with the RFQ commissioning and many thanks also to the workers from Lanzhou Kejin Taiji Corporation., Ltd., who have made great contributions to the copper cavity fabrication. This work was supported by the National Basic Research Program of China (Grant No. 2014CB845503).

[1] J. Knaster, P. Cara, A. Kasughai, Y. Okumura, and M. Sugimoto, Challenges of the high current prototype accelerator of IFMIF/EVEDA, in *Proceedings of the 7th International Particle Accelerator Conference, IPAC-2016, Busan, Korea, 2016* (JACoW, Geneva, Switzerland, 2016), pp. 52–57, http://accelconf.web.cern.ch/AccelConf/ipac2016/papers/mozb02.pdf.

[2] Z. L. Zhang, Y. He, A. M. Shi *et al.*, Design of a four vane RFQ for China ADS project, in *Proceedings of the 26th Linear Accelerator Conference (LINAC-2012), Tel-Aviv, Israel, 2012* (JACoW, Tel Aviv, 2012), pp. 942–944, http://epaper.kek.jp/LINAC2012/papers/thpb039.pdf.

[3] P. Fischer, A. Schempp, and J. Hauser, A CW RFQ accelerator for deuterons, in *Proceedings of the 21st Particle Accelerator Conference, Knoxville, TN, 2005* (IEEE, Piscataway, NJ, 2005), pp. 794–795, http://accelconf.web.cern.ch/AccelConf/p05/PAPERS/RPAP002.PDF.

[4] L. Young, Operations of the LEDA resonantly coupled RFQ, in *Proceedings of the 19th Particle Accelerator Conference, Chicago, IL, 2001* (IEEE, New York, 2001), pp. 309–313, https://doi.org/10.1109/PAC.2001.987501.

[5] Y. He, High intensity RFQs: Review on recent developments, common problems, solutions, in *Proceedings of the 8th International Particle Accelerator Conference, Copenhagen, Demark, 2017*, http://accelconf.web.cern.ch/AccelConf/ipac2017/talks/wexa1_talk.pdf.

[6] F. J. Jia, K. Zhu, Y. R. Lu, Z. Wang, Z. Y. Guo, Q. Fu, and Y. He, Beam Dynamics Design of a 50 mA D+ RFQ, Chin. Phys. Lett. **33**, 072901 (2016).

[7] Q. Fu, K. Zhu, Y. R. Lu, M. J. Easton, S. L. Gao, Z. Wang, F. J. Jia, H. P. Li, P. P. Gan, and Y. He, Design and cold model experiment of a continuous-wave deuteron radio-frequency quadrupole, Phys. Rev. Accel. Beams **20**, 120101 (2017).

[8] V. Andreev *et al.*, First beam test of 81.25 MHz RFQ for ITEP-TWAC, in *Proceedings of the 2nd International Particle Accelerator Conference, San Sebastián, Spain, 2011* (IEEE, San Sebastián, Spain, 2011), pp. 2622–2624, http://accelconf.web.cern.ch/accelconf/IPAC2011/papers/weps056.pdf.

[9] P. N. Ostroumov *et al.*, Development and beam test of a continuous wave radio frequency quadrupole accelerator, Phys. Rev. ST Accel. Beams **15**, 110101 (2012).

[10] A. Perry, C. Dickerson, P. Ostroumov, and G. Zinkann, Beam characterization of a new continuous wave radio frequency quadrupole accelerator, Nucl. Instrum. Methods Phys. Res., Sect. A **735**, 163–168 (2014).

[11] V. Koshelev, Design of 4-vane RFQ with magnetic coupling windows for NUCLOTRON injector LU-20, in *Proceedings of the 28th Linear Accelerator Conference, LINAC-2016 East-lansing, MI, 2016* (JACoW, Geneva, Switzerland, 2016), pp. 575–577, http://accelconf.web.cern.ch/AccelConf/linac2016/papers/tuplr050.pdf.

[12] CST, http://www.cst.com.

[13] R. Duperrier, TOUTATIS: A radio frequency quadrupole code, Phys. Rev. ST Accel. Beams **3**, 124201 (2000).

[14] F. Naito, H. Tanaka, and K. Nanmo, Input coupler of the J-PARC DTL, in *Proceedings of the 26th Linear Accelerator Conference (LINAC-2012), Tel-Aviv, Israel 2012* (JACoW, Tel Aviv, 2012), pp. 690–692, https://accelconf.web.cern.ch/AccelConf/LINAC2012/papers/tupb099.pdf.

[15] P. N. Ostroumov *et al.*, High power test of a 57-MHz CW RFQ, in *Proceedings of the 20th Linear Accelerator Conference (LINAC 2006), Knoxville, TN, 2006,*

THP079, pp. 767–769, http://epaper.kek.jp/l06/PAPERS/THP079.PDF.

[16] J. P. Duke *et al.*, Measurements of rf cavity voltages by x-ray spectrum measurements, in *Proceedings of International Linac Conference, Monterey, CA, 2000, MOC08*, pp. 164–165, http://accelconf.web.cern.ch/AccelConf/l00/papers/MOC08.pdf.

[17] A. P. Zhukov, SNS RFQ voltage measurements using x-ray spectrometer, in *Proceedings of IBIC 2016, Barcelona, Spain, 2016*, pp. 154–165, http://accelconf.web.cern.ch/AccelConf/ibic2016/papers/mopg44.pdf.

[18] D. Uriot and N. Pichoff, TraceWin, documentation, CEA/DSM/DAPNIA/SEA/2000/4 (2000).

[19] R Ferdinand, Commissioning of SPIRAL2 cw RFQ and linac, in *Proceedings of the 8th International Particle Accelerator Conference, Copenhagen, Demark, 2017*, pp. 2462–2465, http://accelconf.web.cern.ch/AccelConf/ipac2017/papers/weoaa1.pdf.

[20] R. Ferdinand, G. Congretel, A. Curtoni *et al.*, SPIRAL2 RFQ design, in *Proceedings of the 9th European Particle Accelerator Conference, Lucerne, 2004* (EPS-AG, Lucerne, 2004), pp. 2026–2028, http://pdfs.semanticscholar.org/c8f9/6e236a323da2c567098928d4797d91dcbc43.pdf.

[21] L. Weissman *et al.*, Installation, high-power conditioning and beam commissioning of the upgraded SARAF 4-rods RFQ, J. Instrum. **13**, T05004 (2018).

[22] L. Bellan, M. Comunian, and E. Fagotti, Beam dynamics of the first beams for IFMIF-EVEDA RFQ commissioning, in *Proceedings of the 9th International Particle Accelerator Conference IPAC2018, Vancouver, BC, Canada*, http://accelconf.web.cern.ch/AccelConf/ipac2018/papers/thpak019.pdf.

[23] E. Fagotti, L. Antoniazzi, L. Bellan *et al.*, Beam commissioning of the IFMIF EVEDA very high power RFQ, in *Proceedings of the 9th International Particle Accelerator Conference IPAC2018, Vancouver, BC, Canada*, http://accelconf.web.cern.ch/AccelConf/ipac2018/papers/thxgbf2.pdf.

[24] W. P. Dou, W. L. Chen, F. F. Wang *et al.*, Beam dynamics and commissioning of cw RFQ for a compact deuteron-beryllium neutron source, Nucl. Instrum. Methods Phys. Res., Sect. A **903**, 85 (2018).